Vol 465|6 May 2010|doi:10.1038/nature09035

LETTERS

Phase-preserving amplification near the quantum limit with a Josephson ring modulator

N. Bergeal[1,2], F. Schackert[1], M. Metcalfe[1,3], R. Vijay[1,4], V. E. Manucharyan[1], L. Frunzio[1], D. E. Prober[1], R. J. Schoelkopf[1], S. M. Girvin[1] & M. H. Devoret[1]

Recent progress in solid-state quantum information processing[1] has stimulated the search for amplifiers and frequency converters with quantum-limited performance in the microwave range. Depending on the gain applied to the quadratures of a single spatial and temporal mode of the electromagnetic field, linear amplifiers can be classified into two categories (phase sensitive and phase preserving) with fundamentally different noise properties[2]. Phase-sensitive amplifiers use squeezing to reduce the quantum noise, but are useful only in cases in which a reference phase is attached to the signal, such as in homodyne detection. A phase-preserving amplifier would be preferable in many applications, but such devices have not been available until now. Here we experimentally realize a proposal[3] for an intrinsically phase-preserving, superconducting parametric amplifier of non-degenerate type. It is based on a Josephson ring modulator, which consists of four Josephson junctions in a Wheatstone bridge configuration. The device symmetry greatly enhances the purity of the amplification process and simplifies both its operation and its analysis. The measured characteristics of the amplifier in terms of gain and bandwidth are in good agreement with analytical predictions. Using a newly developed noise source, we show that the upper bound on the total system noise of our device under real operating conditions is three times the quantum limit. We foresee applications in the area of quantum analog signal processing, such as quantum non-demolition single-shot readout of qubits[4], quantum feedback[5] and the production of entangled microwave signal pairs[6].

In this Letter, we focus on parametric amplifiers that are powered by an a.c. source (the pump) with frequency f_p. Such amplifiers operate with a minimal number of degrees of freedom and are the natural candidates for ultralow-noise operation[7,8]. A single spatial and temporal mode of the electromagnetic field with carrier frequency f can be decomposed into its in-phase quadrature, $A_{||}\cos(2\pi ft)$, and its out-of-phase quadrature, $A_{\perp}\sin(2\pi ft)$. Linear amplifiers can be classified into two categories on the basis of how they treat these two quadratures. On the one hand, a phase-preserving amplifier treats both quadrature components with the same gain ($\sqrt{G}$), as an ordinary operational amplifier would ($A_{||} \rightarrow \sqrt{G}A_{||}$; $A_{\perp} \rightarrow \sqrt{G}A_{\perp}$). On the other hand, in a phase-sensitive amplifier the gains of the quadratures are the reciprocals of each other ($A_{||} \rightarrow \sqrt{G}A_{||}$; $A_{\perp} \rightarrow (1/\sqrt{G})A_{\perp}$). Regarding their noise properties, there is a fundamental difference between these two types of amplifier.

The minimum noise energy added to the input signal by a phase-preserving amplifier is one-half that of a photon at the signal frequency, $hf/2$, where h is Planck's constant[2,9,10]. However, a phase-sensitive amplifier is subject only to a lower limit on the product of the noise added to the two quadratures, and can thus squeeze the quantum noise in one quadrature at the expense of extra noise in the other[2,11]. Although such amplifiers can seem valuable because of their potential ability to operate below the quantum limit, they are only useful in cases in which a reference phase is attached to the signal. For applications in which the information carried by the signal is contained in both quadratures, or, equivalently, in both the amplitude and the phase, a phase-preserving amplifier is preferable. However, so far little attention has been given to intrinsically phase-preserving, non-degenerate parametric amplifiers operating near the quantum limit in the microwave frequency range. They involve two distinct internal resonant modes of the circuit, conventionally called the 'signal', with centre frequency f_s, and the 'idler', whose frequency, f_i, differs from f_s by at least the sum of the bandwidths of the two resonances. This is in contrast with phase-sensitive, degenerate parametric amplifiers, which operate with only one internal resonant mode[12–16]. The challenge of building phase-preserving amplifiers arises from the difficulty of controlling the two modes and coupling them together with the pump.

The circuit we call a Josephson parametric converter (JPC), shown outlined in red in Fig. 1a, was theoretically described in ref. 3. Its operation is based on a novel nonlinear device, the Josephson ring modulator, which consists of four nominally identical Josephson junctions forming a superconducting loop threaded by a magnetic flux, Φ. Two superconducting resonators, A and B, couple to the differential modes of the ring[3]. In the following, f_a and f_b and, respectively, Q_a and Q_b denote the resonant frequencies and quality factors of the corresponding resonators. An additional transmission line carries the pump signal, at frequency f_p, and is weakly coupled to the common mode of the ring through capacitors[3]. From the point of view of the signals, the device has two ports: port 1, driven at frequency f_1, feeds resonator A and port 2, driven at frequency f_2, feeds resonator B. In contrast with previous Josephson parametric amplifiers, we have here a complete separation of the signal and idler modes both spatially and temporally. The JPC can be operated as a phase-preserving amplifier, for $f_p = f_1 + f_2$, or as a unit-photon-gain frequency converter, for $f_p = |f_2 - f_1|$. In this paper, we focus only on the amplification mode, in which case the JPC is described by the input–output relations[3]

$$\hat{a}_1^{\text{out}} = r_1\hat{a}_1^{\text{in}} + s_1\hat{a}_2^{\dagger\text{in}} \quad (1)$$

$$\hat{a}_2^{\text{out}} = r_2\hat{a}_2^{\text{in}} + s_2\hat{a}_1^{\dagger\text{in}} \quad (2)$$

where $\hat{a}_{1(2)}$ and $\hat{a}_{1(2)}^{\dagger}$ are annihilation and, respectively, creation operators at port 1 (frequency f_1) and port 2 (frequency f_2), expressed in units of the square root of photon number per unit time. The superscripts 'in' and 'out' respectively refer to the input and output modes

[1]Department of Physics and Applied Physics, Yale University, New Haven, Connecticut 06520-8284 USA. [2]LPEM-UPR5, CNRS, ESPCI ParisTech, 10 Rue Vauquelin, 75005 Paris, France. [3]The Joint Quantum Institute, University of Maryland, College Park, Maryland 20742, USA. [4]Department of Physics, University of California, Berkeley, California 94720-7300, USA.

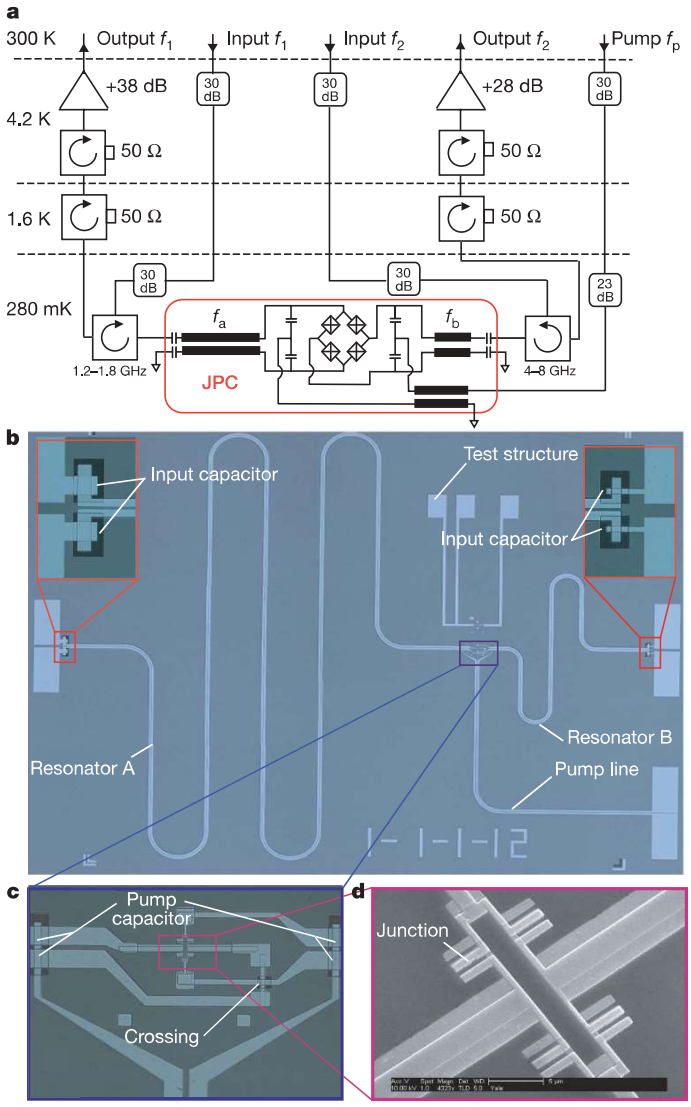

Figure 1 | The JPC and its microwave measurement set-up. a, JPC sample (outlined in red) whose signal ports are connected to two attenuated input lines and two output lines using cryogenic circulators, and whose pump port is fed by a fifth line. The output signals are first amplified by high-electron-mobility transistor (HEMT) cryogenic amplifiers at the 4.2-K stage. Two isolators are placed at the 4.2-K and 1.6-K stages to minimize the back-action of the amplifier on the sample. At room temperature (300-K stage), the signals are further amplified by about 60 dB before being measured. **b**, Optical picture of the JPC. It consists of two coplanar-stripline aluminium resonators respectively 17 and 3.6 mm long coupled to the Josephson ring modulator on one side and to contact pads via input capacitors on the other side. A third coplanar stripline carries the pump signal. The input capacitors are built from two aluminium layers separated by a SiO_x dielectric layer. **c**, Close-up of the connection between the Josephson ring modulator, the resonators and the pump line. The pump is weakly coupled to the resonators through the SiO_x dielectric layer, which provides a small capacitance of order 20 fF. The crossing point of the two resonators is isolated by the same SiO_x layer. **d**, Scanning electron microscope pictures of the Josephson ring modulator showing its four Al/AlO_x/Al junctions. Each junction is surrounded by the two shadow electrodes produced by the Dolan bridge double-angle evaporation technique. The loop of the ring has an area of 3 μm × 17 μm and the junction area is 5 μm × 1 μm.

at each port. Relations (1) and (2) thus determine the properties of the amplifier, including its noise in the quantum limit.

The coefficients r_1, r_2, s_1 and s_2 satisfy the symplectic relations $|r_{1(2)}|^2 - |s_{1(2)}|^2 = 1$. They are given by

$$r_{1(2)} = -\frac{(\vartheta_{2(1)}+i)(\vartheta_{1(2)}+i)-|\rho|^2}{(\vartheta_{2(1)}+i)(\vartheta_{1(2)}-i)-|\rho|^2} \quad (3)$$

$$s_{1(2)} = \frac{-2i\rho}{(\vartheta_{2(1)}+i)(\vartheta_{1(2)}-i)-|\rho|^2} \quad (4)$$

where $\vartheta_{1(2)} = Q_{a(b)}(f_{1(2)}^2 - f_{a(b)}^2)/f_{1(2)}f_{a(b)}$. We have also introduced the dimensionless pump current

$$|\rho| = \frac{1}{4}\sqrt{Q_a Q_b p_a p_b}\,\frac{I_p}{I'_0} \quad (5)$$

where I_p is the pump current, I'_0 is the pump-mode critical current and $p_{a(b)} = L_J/(L_J + L_{a(b)})$ are the participation ratios of the inductance of the Josephson ring modulator, L_J, in series with the resonator inductances, $L_{a(b)}$ (ref. 3). At resonant tuning ($f_1 = f_a$ and $f_2 = f_b$), the expressions for the coefficients reduce to $r_1 = r_2 = \sqrt{G} = (1+|\rho|^2)/(1-|\rho|^2)$ and $|s_1| = |s_2| = \sqrt{G-1} = 2|\rho|/(1-|\rho|^2)$. The symbol G refers to the power gain at the band centre, which also characterizes the gain of the temporal mode defined by the bandwidth of the amplifier.

The diagonal terms, r_1 and r_2, should be understood as a photon '*cis*-gain' (or return gain), characteristic of the one-port reflection amplifier operation: the incoming wave at either port is reflected with a power gain of $|r_1|^2$ or $|r_2|^2$, as appropriate, and its phase is preserved. The non-diagonal terms, s_1 and s_2, should be understood as a photon '*trans*-gain' (or through gain) from one port to the other, and describe the behaviour of a frequency converter ($f_1 \rightarrow f_2$ or $f_2 \rightarrow f_1$) with power gain $|s_{1(2)}|^2 = |r_{1(2)}|^2 - 1$. The possibility of performing the important function of up- and down-conversion is another feature that distinguishes the non-degenerate parametric amplifier from the degenerate one. It arises from the presence in the circuit of two different spatial modes with different frequencies, whose sum is equal to the pump frequency. The *cis*-gain and *trans*-gain can be varied simply by changing the pump power characterized by the parameter $|\rho|$: $|r_{1(2)}| \approx |s_{1(2)}| \rightarrow \infty$ as $|\rho| \rightarrow 1^-$.

Figure 1b–d shows pictures of our JPC sample made of aluminium on a silicon wafer, using a three-step fabrication process combining optical and electron-beam lithography (Methods). After fabrication, the JPC chip is mounted on a microwave circuit board and housed in a copper sample box equipped with a superconducting coil. The sample box is anchored to the 280-mK cold stage of a ^{3}He refrigerator and placed in a combination of magnetic and superconducting shield. Our measurement set-up is shown schematically in Fig. 1a. In this arrangement, the incoming noise at the input ports of the JPC arises from the 50-Ω resistance presented by the last attenuator in the input lines. The characteristics of the resonators are given in Supplementary Information. In the following, we will focus on measurements performed at the bias point $\Phi = \Phi_0/2$ (Φ_0, flux quantum), where $f_a = 1.631$ GHz, $f_b = 7.219$ GHz, $Q_a = 450$ and $Q_b = 120$.

We operated the device in amplification mode by feeding the pump line with a continuous microwave signal at a fixed frequency, $f_p = f_a + f_b = 8.85$ GHz. Figure 2a shows the gain curves $|r_1|^2$ and $|r_2|^2$ measured at the corresponding ports for different values of the pump power. They are symmetrically centred on the resonance frequencies f_a and f_b and, importantly, the symmetry of the ring modulator is such that they do not shift noticeably with the pump power, unlike in other Josephson parametric amplifiers[12–14]. In addition to the experimental data, we also plot the theoretical expression in equation (3) for $|r_1|^2$ and $|r_2|^2$ as a function of drive frequencies f_1 and f_2, using the measured values of f_a, f_b, Q_a and Q_b. Data and theory are in very good agreement up to 40 dB. It is remarkable that only one adjustable parameter, $|\rho|$, is sufficient to capture the whole shape of each gain curve. In particular, the relationship between bandwidth, B, and gain, $B = (2/\sqrt{G})(Q_a/f_a + Q_b/f_b)^{-1}$, is well satisfied[3].

A similar agreement with theory is also obtained for the phases of the complex gains r_1 and r_2, as shown in the Supplementary Fig. 2. As far as the relationship between $|\rho|$ and I_p is concerned, we found experimentally that, for a wide range of gains, $|\rho| \propto \log(I_p)$. This dependence differs from the linear relation, equation (5), obtained in the framework of ref. 3 assuming a stiff pump, which describes an

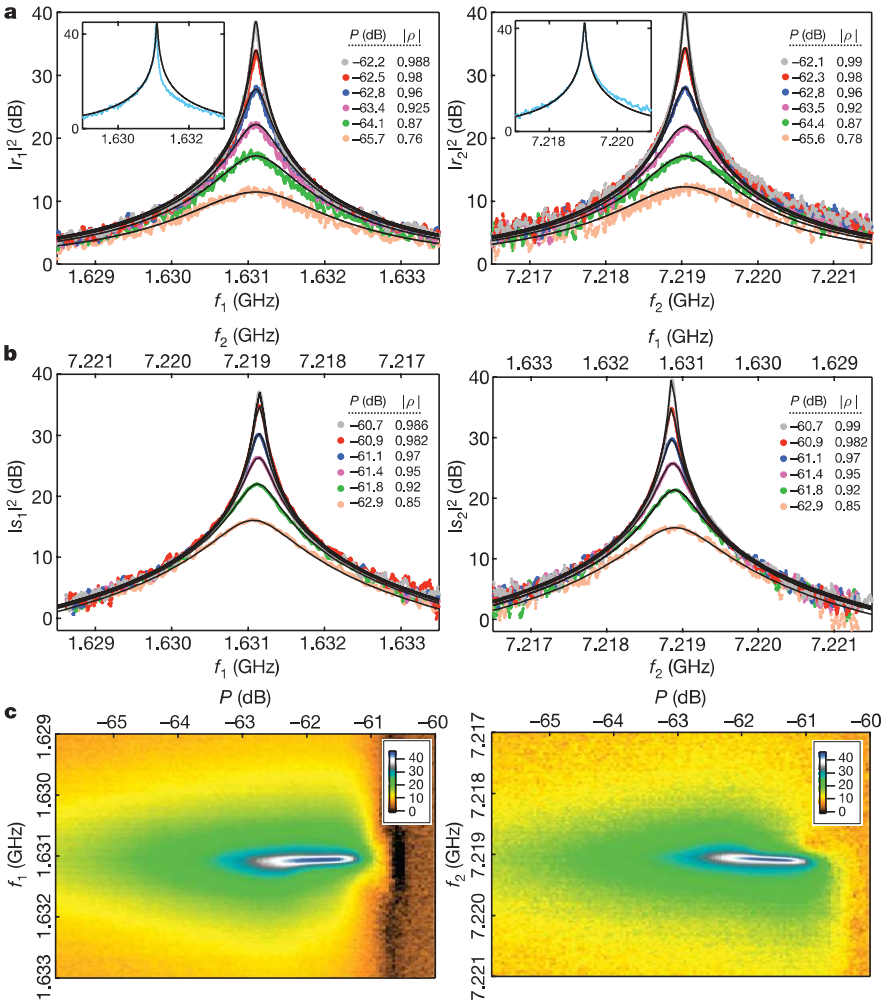

Figure 2 | Gain of the JPC. **a**, Power *cis*-gain of the JPC as a function of the input signal frequency, for different values of the pump power, P, measured at port 1 (left) and port 2 (right). The solid lines correspond to the theoretical expressions for $|r_1|^2$ and $|r_2|^2$ (equation (3)) obtained for the indicated values of the fit parameter, $|\rho|$. Inset, curves obtained at higher gain. The fits correspond to $|\rho| = 0.994$ (left) and $|\rho| = 0.992$ (right). **b**, Photon *trans*-gain of the JPC as a function of the input signal frequency (bottom axis) and the converted frequency (top axis), measured between port 1 and port 2 (left) and between port 2 and port 1 (right) for different values of the pump power. The solid lines correspond to the theoretical expressions for $|s_1|^2$ and $|s_2|^2$ (equation (4)) obtained for the indicated values of $|\rho|$. **c**, Photon *cis*-gain of the JPC plotted (colour, dB) as a function of the drive frequencies and the pump power measured at port 1 (left) and port 2 (right). The data shown in **a**, **b** and **c** correspond to different runs.

ideal situation imperfectly realized here because the common-mode impedance increases with gain. When the gain is further increased to a maximum of 44 dB, the curves deviate from the model as shown in the insets of Fig. 2a, indicating that saturation effects are becoming important, as discussed below. These effects occur within a fraction of a per cent from the theoretical onset of self-oscillations of the system, which corresponds to $|\rho| = 1$. Moreover, as shown in Fig. 2c, after reaching its maximum value the gain starts to decrease when the pump power is further increased, and finally vanishes rapidly when the critical current of the junctions is reached. The non-observation of parametric self-oscillations is due to the saturation of the device by the signal resulting from the amplification of the noise, when its peak current amplitude reaches the critical current.

In practice, an amplifier must have a minimum gain to overcome the noise of the following amplifier in the measurement chain. Assuming the best state-of-the-art commercial device to be a following amplifier with a noise temperature of a few kelvins, we are led to a requirement of at least 20 dB of power gain, which the present JPC satisfies by a comfortable margin. This is in contrast with recent results obtained with other parametric amplifiers[12,13] or with d.c. microwave amplifiers based on superconducting interference devices[17–19] working in the same frequency range. We believe that the differences in gain performances between our JPC and other Josephson amplifiers originate in the purity of the three-waves mixing of signal, idler and pump offered by the ring modulator. Indeed, the observed maximum gain is compatible with the order-of-magnitude theoretical prediction given by[3]

$$G < \frac{I_0}{2\pi e(p_a f_a + p_b f_b)}$$

where e is the fundamental charge, $I_0 = 5 \pm 1\ \mu A$, $p_a(I_0) = 0.012$ and $p_b(I_0) = 0.055$. The same consideration based on the maximum output power that the Josephson ring modulator can deliver also explains the dynamic range of our amplifier (Supplementary Fig. 3).

In addition to the one-port amplifier operation, corresponding to the diagonal terms r_1 and r_2, the JPC also performs two-port frequency conversion with gain, corresponding to the non-diagonal terms s_1 and s_2. Figure 2b shows the typical gain curves measured between the two ports both for up-conversion ($f_1 \rightarrow f_2$) and for down-conversion ($f_2 \rightarrow f_1$). As for $|r_1|^2$ and $|r_2|^2$, we obtain excellent agreement with the theoretical expressions for $|s_1|^2$ and $|s_2|^2$. In Fig. 3, we show that we can adjust the centre frequency of the signal band by detuning the pump frequency. Thus, the tuning bandwidths are found to be given by the intrinsic resonator bandwidths, f_a/Q_a and f_b/Q_b, as expressions (3) and (4) predict. For the high-frequency port of our device, there is a ratio of 95 between the tuning and signal bandwidth if we limit the gain to 20 dB. For the low-frequency port, this ratio is much smaller (5.7) because $f_a/Q_a \ll f_b/Q_b$. Finally, we

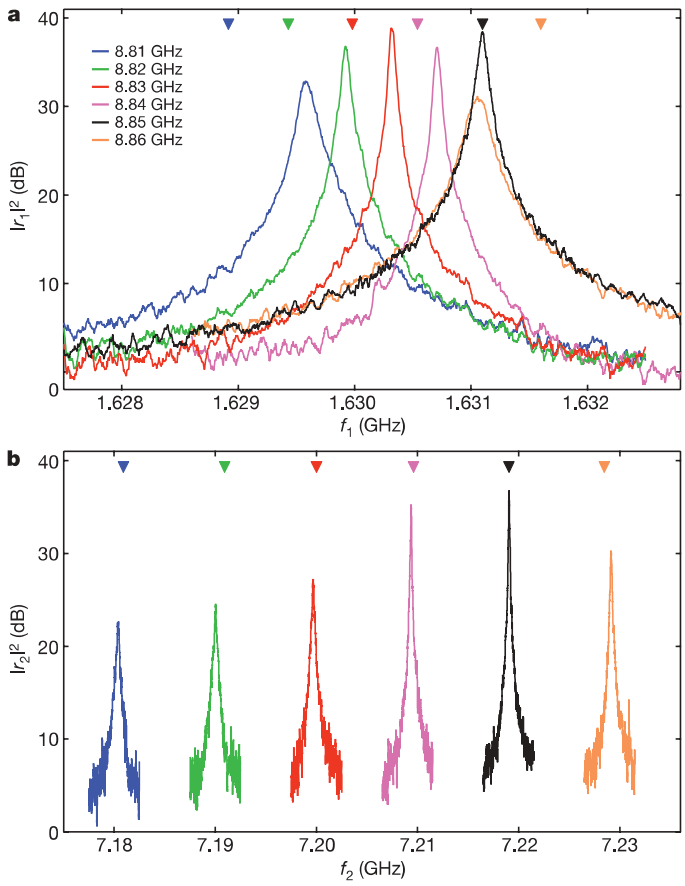

Figure 3 | Tuning the bandwidth of the JPC. *Cis*-gains $|r_1|^2$ (**a**) and $|r_2|^2$ (**b**) as functions of the corresponding drive frequency, for different values of the pump frequency, f_p, as indicated. The pump amplitude has been adjusted at each frequency for optimal gain. The triangular symbols indicate the theoretical location of the centre frequency.

note that the relatively small signal bandwidth of the present device is due to the small intrinsic bandwidth of the low-frequency resonator and could be greatly enhanced by increasing its coupling capacitance and the working frequency. The optimum bandwidth configuration is when the signal and idler bandwidths are equal.

We measured the noise temperature of the JPC using a newly developed noise source based on the hot-electron shot noise regime of a resistor with resistance $R = 50 \pm 1\,\Omega$ (Methods and Supplementary Fig. 4). The temperature of the source is determined by a voltage, $V = RI_{dc}$, across the resistor, where I_{dc} is the bias current. Figure 4a shows the noise on a decibel scale as a function of the frequency f_1 and the voltage V, with the gain of the JPC set to 30 dB. Cuts of the data at $V = 0\,\mu V$ and $V = 85\,\mu V$ are shown in Fig. 4b. Figure 4c shows the noise averaged over a 1-MHz band around the resonance frequency. In the same figure, we compare the data with the theoretical expression

$$S^{th} = G_t(S^{ns}(V,f_1) + S^{add})$$

where G_t is the total gain of the measurement chain, S^{ns} is the noise produced by the noise source (Methods) and S^{add} is the noise added by the amplifier.

For a perfect quantum-limited amplifier, $S^{add} \equiv S^{QL} = hf_1/2$, which corresponds to the noise added by the idler when the load at port 2 is at a temperature, T_0, such that $hf_2 \gg k_B T_0$, where k_B is Boltzmann's constant. We note that although the vertical axis in Fig. 4c is the total noise of the system, it essentially coincides with the output noise of the JPC because the noise added by the following

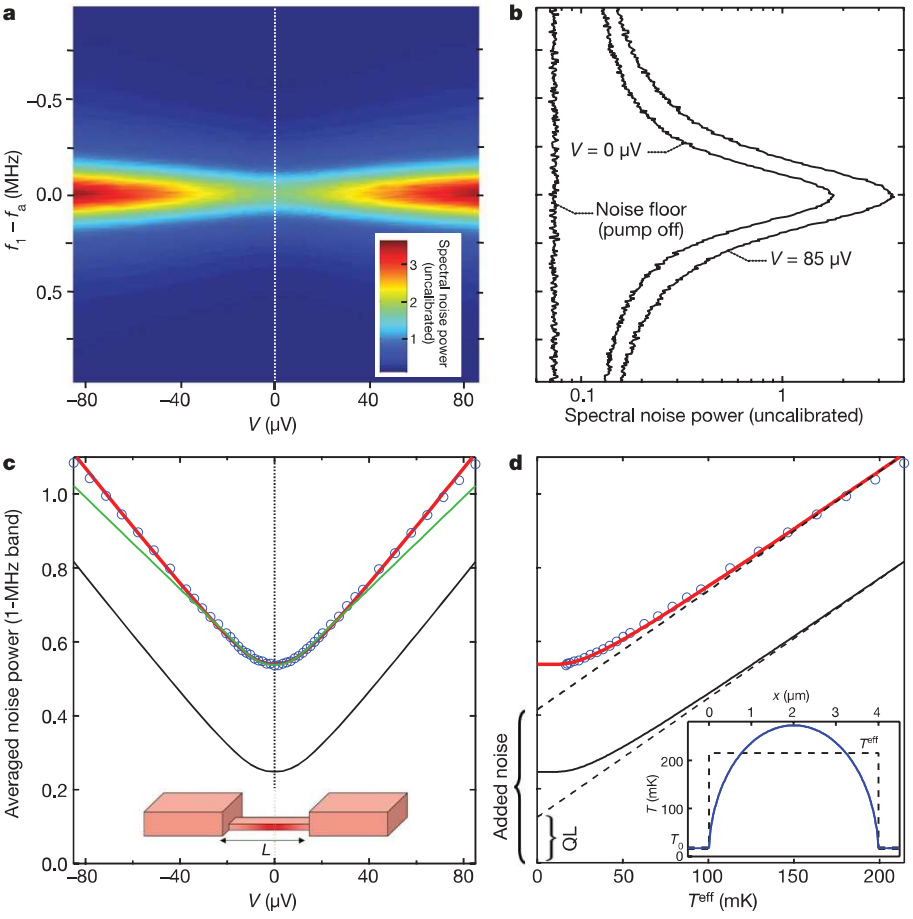

Figure 4 | Noise measurement of the JPC for a 30-dB gain. **a**, Spectral noise power at the output of port 1 (colour) as a function of frequency and voltage across the resistor. **b**, Cuts of the spectral noise power corresponding to $V = 0\,\mu V$ and $V = 85\,\mu V$. The noise floor obtained with the pump off is given as reference. **c**, Noise power at the output of port 1 (open dots; same units as in **a**), averaged over a 1-MHz band around f_a, as a function of the voltage across the resistor. Red line, theoretical expression (equation (6) in Methods) with fitted added noise; green line, same as red line but assuming quantum shot noise for the resistor; black line, theoretical expression (6) plus an ideal quantum-limited amplifier. Inset, schematic of the resistor embedded in its thick and wide thermal reservoirs. **d**, Same as **c** but with the voltage axis converted into the effective temperature of the noise source, T^{eff}. The dashed lines indicate asymptotes of the high-temperature variation. Also shown in this panel is the total added noise power of the system and the ideal case of the quantum limit (QL). Inset, temperature variation profile inside the resistor (Methods).

stages is 17 dB lower, as shown in Fig. 4b. There is a good agreement between theory and experimental data if $S^{add} = 3.37S^{QL}$ (Fig. 4c, red curve). For comparison, we also plot the theoretical result corresponding to the ideal case of a perfect nanowire and a perfect amplifier (Fig. 4c, black curve). The quality of the fit confirms that the resistor is well within the hot-electron regime. For instance, the expression for quantum shot noise (Fig. 4c, green curve; see Methods) cannot be reconciled with the experimental data. In Fig. 4d, the voltage axis has been converted into a temperature scale using the expression for T^{eff} (Methods). The noise added by the amplifier is the vertical intercept of the dashed line corresponding to the asymptotic variation of noise with temperature. Converting the added noise S^{add} into system noise temperature yields $T_N = 125$ mK, which makes the JPC 20–40 times better than the best commercial HEMT amplifier. We attribute the difference between the system noise temperature and the ideal quantum limit, $T_N = 37$ mK, to incomplete isolation of the JPC from spurious noise coming through the post-amplifiers and possibly to imperfections in the line connecting the nanowire to the JPC, which incorporates a circulator and a bias tee.

In conclusion, we have implemented and demonstrated the operation of a new phase-preserving amplifier, the Josephson parametric converter, whose main element is the nonlinear, non-dissipative inductance of a Josephson ring modulator. Our gain, bandwidth and dynamic range results can be understood quantitatively using a simple analytical model involving a minimal number of parameters. We have achieved a power gain amplification of at least 40 dB, which could allow for practical applications such as single-photon detection based on microwave readout[20] or applications involving the measurement of very low microwave power in a limited bandwidth. Our device is also useful as a frequency up-converter or down-converter. Using a newly developed self-calibrating noise source, we obtained an upper bound on the noise added by the JPC that is three times the quantum limit. Extrapolating the present results to devices with resonators having larger bandwidths and higher centre frequencies, we should be able to build a quantum-limited amplifier with 20-dB gain in a 10-MHz bandwidth around 10 GHz, thus allowing dispersive single-shot read out of solid-state qubits[4,21–23] with an irradiation of only a few photons. Our results also open the way for the production of entangled microwave signal pairs by means of two-mode squeezing[6].

METHODS SUMMARY

Fabrication of the device. We first defined the coplanar-stripline resonators and the bottom layers of the input capacitors by evaporating a 110-nm-thick aluminium layer through an optical resist. Then a 270-nm-thick SiO_x layer was deposited through a second optical resist to form the dielectric layers of the different capacitors. Finally, a 240-nm-thick aluminium layer was evaporated to form the pump line and the top layers of the input capacitors. We integrated the Josephson ring modulator using electron-beam lithography and the Dolan bridge double-angle evaporation technique. The nominal size of each junction was $5 \times 1\ \mu m^2$, corresponding to critical currents in the range 3–6 μA, depending on oxidation conditions.

Noise measurements of the JPC. We performed the noise measurements in a dilution refrigerator with a base temperature of $T_0 = 17$ mK, using the hot-electron shot noise produced by a mesoscopic resistor with $R = 50\ \Omega$ embedded in a microwave transmission line. When the resistor is biased with a d.c. current, I_{dc}, an equilibrium electronic temperature profile establishes itself over its length, corresponding to an effective temperature of

$$T^{eff} = \frac{T_0}{2}\left[1 + \left(\nu + \frac{1}{\nu}\right)\arctan(\nu)\right]$$

where $\nu = (\sqrt{3}/2\pi)(eV/k_B T_0)$ and $V = RI_{dc}$ is the voltage across the resistor. The Johnson noise power spectral density produced by the resistor was thus

$$S^{ns}(f,V) = \frac{hf}{2}\coth\left(\frac{hf}{2k_B T^{eff}(V)}\right)$$

We connected the noise source to the input port of the JPC through a bias tee and acquired the output noise as a function of I_{dc} using a spectrum analyser.

Full Methods and any associated references are available in the online version of the paper at www.nature.com/nature.

Received 7 December 2009; accepted 17 March 2010.

1. Clarke, J. & Wilhelm, F. K. Superconducting quantum bits. *Nature* **453,** 1031–1042 (2008).
2. Caves, C. M. Quantum limits on noise in linear amplifiers. *Phys. Rev. D* **26,** 1817–1839 (1982).
3. Bergeal, N. *et al.* Analog information processing at the quantum limit with a Josephson ring modulator. *Nature Phys.* **6,** 296–302 (2010).
4. Lupaşcu, A. *et al.* Quantum non-demolition measurement of a superconducting two-level system. *Nature Phys.* **3,** 119–125 (2007).
5. Ahn, C., Doherty, A. C. & Landahl, A. J. Continuous quantum error correction via quantum feedback control. *Phys. Rev. A* **65,** 042301 (2002).
6. Marquardt, F. Efficient on-chip source of microwave photon pairs in superconducting circuit QED. *Phys. Rev. B* **76,** 205416 (2007).
7. Louisell, W. H., Yariv, A. & Siegman, A. E. Quantum fluctuations and noise in parametric processes. I. *Phys. Rev.* **124,** 1646–1654 (1961).
8. Gordon, J. P., Louisell, W. H. & Walker, L. R. Quantum fluctuations and noise in parametric processes. II. *Phys. Rev.* **129,** 481–485 (1963).
9. Haus, H. A. & Mullen, J. A. Quantum noise in linear amplifiers. *Phys. Rev.* **128,** 2407–2413 (1962).
10. Clerk, A. A., Devoret, M. H., Girvin, S. M., Marquardt, F. & Schoelkopf, R. J. Introduction to quantum noise, measurement and amplification. *Rev. Mod. Phys.* (in the press); preprint at ⟨http://arxiv.org/abs/0810.4729⟩ (2008).
11. Castellanos-Beltran, M. A., Irwin, K. D., Hilton, G. C., Vale, L. R. & Lehnert, K. W. Amplification and squeezing of quantum noise with a tunable Josephson metamaterial. *Nature Phys.* **4,** 928–931 (2008).
12. Castellanos-Beltran, M. A. & Lehnert, K. W. Widely tunable parametric amplifier based on a superconducting quantum interference device array resonator. *Appl. Phys. Lett.* **91,** 083509 (2007).
13. Yamamoto, T. *et al.* Flux-driven Josephson parametric amplifier. *Appl. Phys. Lett.* **93,** 042510 (2008).
14. Yurke, B. *et al.* Observation of parametric amplification and deamplification in a Josephson parametric amplifier. *Phys. Rev. A* **39,** 2519–2533 (1989).
15. Yurke, B. Observation of 4.2-K equilibrium-noise squeezing via a Josephson-parametric amplifier. *Phys. Rev. Lett.* **60,** 764–767 (1988).
16. Movshovich, R. *et al.* Observation of zero-point noise squeezing via a Josephson-parametric amplifier. *Phys. Rev. Lett.* **65,** 1419–1422 (1990).
17. André, M.-O., Mück, M., Clarke, J., Gail, J. & Heiden, C. Radio-frequency amplifier with tenth-kelvin noise temperature based on a microstrip direct current superconducting quantum interference device. *Appl. Phys. Lett.* **75,** 698–700 (1999).
18. Spietz, L., Irwin, K. & Aumentado, J. Input impedance and gain of a gigahertz amplifier using a dc superconducting quantum interference device in a quarter wave resonator. *Appl. Phys. Lett.* **93,** 082506 (2008).
19. Kinion, D&. Clarke, J. Microstrip superconducting quantum interference device radio-frequency amplifier: scattering parameters and input coupling. *Appl. Phys. Lett.* **92,** 172503 (2008).
20. Santavicca, D. F. *et al.* Energy resolution of terahertz single-photon-sensitive bolometric detectors. *Appl. Phys. Lett.* **96,** 083505 (2010).
21. Wallraff, A. *et al.* Strong coupling of a single photon to a superconducting qubit using circuit quantum electrodynamics. *Nature* **431,** 162–167 (2004).
22. Manucharyan, V. E. & Koch, J. Glazman, L. I. & Devoret, M. H. Single Cooper-pair circuit free of charge offsets. *Science* **326,** 113–116 (2009).
23. Mallet, F. *et al.* Single-shot qubit readout in circuit quantum electrodynamics. *Nature Phys.* **5,** 791–795 (2009).

Supplementary Information is linked to the online version of the paper at www.nature.com/nature.

Acknowledgements We thank B. Abdo for his reading of the manuscript. This work was supported by the US National Security Agency through the US Army Research Office grant W911NF-05-01-0365, the W. M. Keck Foundation, and the US National Science Foundation through grant DMR-032-5580. M.H.D. acknowledges partial support from the College de France and from the French Agence Nationale de la Recherche.

Author Contributions N.B. and L.F. fabricated the device. N.B., assisted by F.S. and M.M., performed the measurements. N.B. and M.H.D. carried out the analysis of the results and wrote the paper. R.V., V.E.M., R.J.S. and S.M.G. contributed extensively to discussions of the results. D.E.P. suggested the hot-electron noise source for calibration. R.J.S. contributed through his knowledge of ultralow-noise microwave circuits and measurements.

Author Information Reprints and permissions information is available at www.nature.com/reprints. The authors declare no competing financial interests. Readers are welcome to comment on the online version of this article at www.nature.com/nature. Correspondence and requests for materials should be addressed to N.B. (nicolas.bergeal@espci.fr) or M.H.D. (michel.devoret@yale.edu).

METHODS

Fabrication of the device. Each quarter-wave resonator was built from a coplanar-stripline structure consisting of two 15-μm-wide parallel lines separated by a 4-μm gap. In the first step of fabrication, a 110-nm-thick aluminium layer was evaporated onto a high-resistivity silicon wafer through an optical bilayer resist. A sloped edge was obtained by tilting the sample holder at an angle of 4° and rotating the stage at a speed of $10^{\circ}\,s^{-1}$ during the evaporation. This process defines the coplanar-stripline resonators and the bottom layer of the input capacitors. Then a 270-nm-thick SiO_x layer was deposited through a second optical resist to form, in a single step, the dielectric layer of the input capacitors, the pump coupling capacitors and the insulating layer at the crossing of the two resonator lines. Finally, a second layer of aluminium (240 nm) was evaporated to form the pump line, the top layer of the input capacitors connected to contact pads and the bridge on top of the isolation.

Following the optical processes, the wafer was diced into 50 chips of size 5 mm × 4 mm. Then the Josephson ring modulator was integrated into the device using a MMA/PMMA resist bilayer, electron-beam lithography and the Dolan bridge double-angle evaporation technique. Gentle milling using a hollow-cathode ion gun was used between deposition of metallic layers. The nominal size of each junction is 5 μm × 1 μm. They have nominally identical critical currents with values in the range of 3–6 μA, depending on oxidation conditions. Tests have shown that these values vary from one junction of the ring to another by less than 5%. Although similar embeddings of microampere-critical-current junctions inside microwave resonators have recently been used for bifurcation read out of qubits[24,25] and radio-frequency magnetometry[26], the ring modulator device investigated here works in the weakly nonlinear regime, with the pump amplitude well below the bifurcation threshold. In other words, the currents in the ring modulator remain small enough that only second-order correction of the Josephson inductance needs to be considered in the circuit analysis.

Noise measurement with a mesoscopic resistor. To measure the noise of the JPC, we have developed a source of noise based on the hot-electron shot noise regime of a $R = 50 \pm 1\,\Omega$ mesoscopic copper resistor of length $L = 4\,\mu m$ embedded between two cold reservoirs of temperature $T_0 = 17\,mK$ (Fig. 4c, inset). It is inspired by previous work in which this system was used to calibrate an infrared photon detector[27]. A metallic resistor has several regimes of shot noise depending on the relation between its length, L, and the characteristic length scales involved in the motion of electrons[28]. In the regime where L is greater than the inelastic electron scattering length, L_{e-e}, but shorter than the electron–phonon interaction length L_{e-ph}, the electrons travelling through the resistor redistribute the excess kinetic energy gained from the voltage through electron–electron interactions only[28]. The cooling of the electron system thus occurs only by diffusion to the cold reservoirs and is controlled by the Wiedemann–Franz law. As a result, an equilibrium electronic temperature profile establishes itself over the length of the microbridge[29] (Fig. 4d, inset):

$$T(x) = T_0\sqrt{1+\frac{x}{L}\left(1-\frac{x}{L}\right)\frac{3e^2V^2}{\pi^2k_B^2T_0^2}}$$

The effective electronic temperature of the nanowire is given by integrating over its length:

$$T^{eff} = \frac{1}{L}\int_0^L T(x)\,dx = \frac{T_0}{2}\left[1+\left(\nu+\frac{1}{\nu}\right)\arctan(\nu)\right]$$

Here $\nu = (\sqrt{3}/2\pi)(eV/k_BT_0)$, k_B is Boltzmann's constant and $V = RI_{dc}$ is the voltage across the resistor. Thus, T^{eff} is a function only of V, T_0 and fundamental constants, hence the interest of this noise source. The Johnson noise power spectral density produced by the resistor is approximately given by

$$S^{ns}(f,V) = \frac{hf}{2}\coth\left(\frac{hf}{2k_BT^{eff}(V)}\right) \quad (6)$$

For $k_BT^{eff} \gg hf$, this expression reduces to the well-known classical Johnson noise power spectral density, k_BT^{eff}. We have verified that computing the shot noise of the resistor using equation (6) yields the same result, at the percentage precision level, as when the full space-dependent spectral density of noise is taken into account.

This noise source has the following advantages: there is no macroscopic heating of the sample and thus no perturbation of the JPC operating point; it is self-calibrating; it has a response time in the microsecond range[27]; and it is controlled using a d.c. current, I_{dc}. Our 50-Ω copper nanowire resistor is 4 μm long, 80 nm wide, and 20 nm thick. Using a double-angle evaporation technique, the resistor was embedded into a 500-nm-thick 50-Ω CPW transmission line of 400-μm width on each side, forming good thermal reservoirs. The noise source chip was bonded with gold wire on a sample holder. In this experiment, both the noise source and the JPC were anchored to the mixing chamber of a dilution refrigerator with a base temperature of $T_0 = 17\,mK$ (Supplementary Fig. 4). According to previous studies[30], the 4-μm length ensures that the resistor is in the hot-electron regime, $L_{e-e} < L < L_{e-ph}$, at the working temperature. The sample holder was connected to the high-frequency port of a bias tee. Direct current was applied to the noise source using a cold current divider connected to the d.c. port of the bias tee. Finally, the d.c.-blocked high-frequency port of the bias tee was connected to port 1 of the JPC by a circulator.

24. Metcalfe, M. *et al.* Measuring the decoherence of a quantronium qubit with the cavity bifurcation amplifier. *Phys. Rev. B* **76,** 174516 (2007).
25. Boulant, N. *et al.* Quantum nondemolition readout using a Josephson bifurcation amplifier. *Phys. Rev. B* **76,** 014525 (2007).
26. Vijay, R., Devoret, M. H. & Siddiqi, I. The Josephson bifurcation amplifier. *Rev. Sci. Instrum.* **80,** 111101 (2009).
27. Prober, D. E. *et al.* Ultrasensitive quantum-limited far-infrared STJ detectors. *IEEE Trans. Appl. Superconduct.* **17,** 241–245 (2007).
28. Steinbach, A. H., Martinis, J. M. & Devoret, M. H. Observation of hot-electron shot noise in a metallic resistor. *Phys. Rev. Lett.* **76,** 3806–3809 (2004).
29. Nagaev, K. E. Influence on electron-electron scattering on shot noise in diffusive contact. *Phys. Rev. B* **52,** 4740–4743 (1995).
30. Pothier, H., Gueron, S., Birge, N. O., Esteve, D. & Devoret, M. H. Energy distribution function of quasiparticles in mesoscopic wires. *Phys. Rev. Lett.* **79,** 3490–3493 (1997).